Interplay between topography, fog and vegetation in the central South Arabian mountains revealed using a novel Landsat fog detection technique

Lawrence Ball[a] and Joseph Tzanopoulos[b]

A. **(Corresponding Author) Department of Evolution, Ecology and Organismal Biology, The Ohio State University, Columbus, OH 43210, USA. ball.2174@osu.edu**
B. **Durrell Institute of Conservation and Ecology, School of Anthropology and Conservation, University of Kent, Canterbury CT27NR, UK. j.tzanopoulos@kent.ac.uk**

Running title: Topography-fog-vegetation analysis in south Arabia

Word count: Abstract: 205, main text: 5000, acknowledgements: 24, references: 1884, table and figure legends: 576.

Number of tables and figures: One table and ten figures.

Abstract

In the central South Arabian mountains of Yemen and Oman, monsoon fog interception by the endemic cloud forest is essential for ecosystem functions and services. Yet, we know little about the local factors affecting fog distributions and their cumulative effects on vegetation. To examine these relationships, we developed a novel method of high-resolution fog detection using Landsat data, and validated the results using occurrence records of eight moisture-sensitive plant species. Regression tree analysis was then used to examine the topographic factors influencing fog distributions and the topoclimatic factors influencing satellite-derived vegetation greenness. We find that topography affects fog distributions. Specifically, steep windward slopes obstruct the inland movement of fog, resulting in heterogenous fog densities and hotspots of fog interception. We find that fog distributions

explain patterns of vegetation greenness, and overall, that greenness increases with fog density. The layer of fog density describes patterns of vegetation greenness more accurately than topographic variables alone, and thus, we propose that regional vegetation patterns more closely follow a fog gradient, than an altitudinal gradient as previously supposed. The layer of fog density will enable an improved understanding of how species and communities, many of which are endemic, range-restricted, and in decline, respond to local variability in topoclimatic conditions.

Keywords: topography, fog, vegetation, regression tree analysis (RTA), central South Arabian mountains (CSAM), Dhofar Oman, Mahra Yemen, monsoon, khareef, Anogeissus dhofarica, cloud forest, Normalized Difference Vegetation Index (NDVI)

1. Introduction

Fog is an important hydrologic input in many ecosystems around the world (Bruijnzeel et al., 2005). Fog interception by vegetation is the main process by which fog moisture and the nutrients it contains can enter an ecosystem, in addition to simple deposition (Weathers et al., 2006). In arid environments, particularly in coastal and montane locations, fog can supply a large part of the water balance. Water is often the primary limiting factor to vegetation growth and vegetation responses to fog are usually more pronounced than in areas with high rainfall (Hildebrandt et al., 2007). The spatial distribution of fog is often strongly affected by topography (Gultepe et al., 2007; Bruijnzeel et al., 2005). In turn, the distribution of fog can affect vegetation patterns (Scholte and De Geest, 2010; Martorell and Ezcurra, 2002; Cavelier and Guillermo, 1989; Hildebrandt and Eltahir, 2008). These relationships can underpin the ecohydrology in arid environments and provide a crucial freshwater source for people and nature. However, few studies have examined the interplay between topography, fog and vegetation at the landscape scale, although overlay analysis of these biospheric components has been used to predict tropical cloud forest distributions (Mulligan, 2010). In this study, we use a novel high-resolution fog detection technique, a suite of geospatial datasets, and regression tree analysis to examine the interplay between topography, fog and vegetation in the central South Arabian mountains.

The central South Arabian mountains (CSAM) are located in the Mahra Governorate of Yemen and the Dhofar Governorate of Oman (Figure 1). They receive very dense fogs (visibility < 100 m) during the monsoon, popularly known as the khareef. From mid-June to mid-September, south-westerly winds cause an upwelling of cold sea water off the coast, lowering the sea temperature to c. 18 degrees. As warm moist winds blow over it, advection fogs form and build up against the south-facing mountain escarpments (Stanley Price et al., 1988; Ghazanfar and Fisher, 1998). A temperature inversion, caused by warm northerly winds from the desert, limits the inland movement of fog (Kürschner et al., 2004; Friesen et al., 2018).

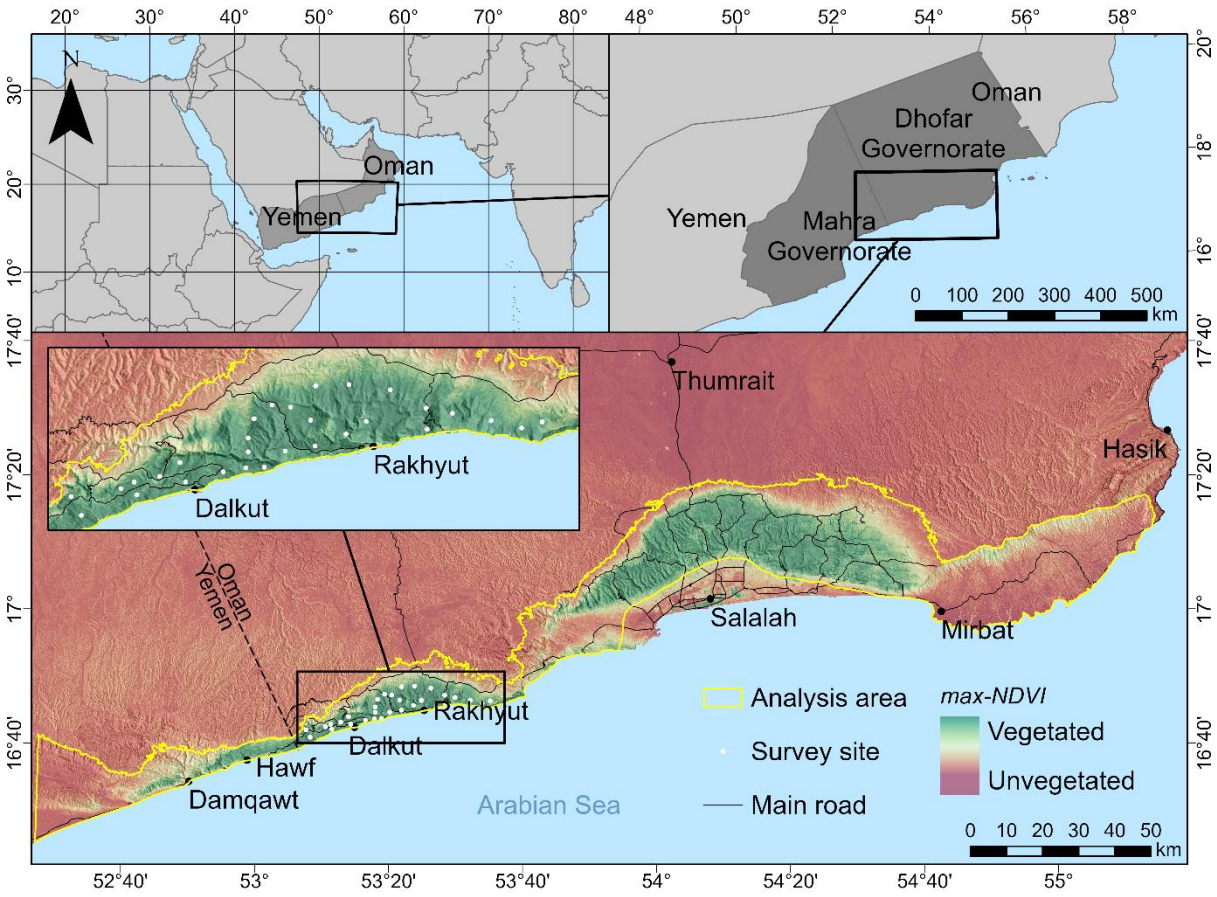

Figure 1. A map of the central South Arabian mountains in the Dhofar Governorate of Oman and the Mahra Governorate of Yemen, and their location in the Arabian Peninsula. The regression tree analysis (RTA) area, and the 2016 botanical survey sites, are shown.

The monsoon fogs support the *Hybantho durae-Anogeissetum dhofaricae,* a drought deciduous cloud forest community (Kürschner et al., 2004). It is endemic to the CSAM and the remnants of a once continuous paleo-African flora (Meister et al., 2005). It comprises at least 262 floral species, many of which are endemic to the CSAM (Patzelt, 2015). The cloud forest is interspersed with grasslands dominated by *Arthraxon junnarensis*, *Apluda mutica* and *Themeda quadrivalvis*, and shrublands, such as the *Euphorbia balsamifera* cushion shrub community which occupies the high-altitude fringes of the monsoon zone (Patzelt, 2011, 2015). Fog interception by the cloud forest is estimated to contribute as much water as rainfall (mean annual precipitation is 200 mm) to net precipitation (Hildebrandt et al., 2007). The quantity of fog water intercepted by the locally dominant and endemic tree,

Anogeissus dhofarica (250% more than rainfall), is amongst the highest recorded for any tree species (Friesen et al., 2018). In addition, the fog cover greatly reduces solar radiation and increases humidity, lowering evapotranspiration rates, enabling deep infiltration and storage of soil water, which is then used by the plants to extend the growing season for a further three months after the monsoon (Hildebrandt and Eltahir, 2007; Bruijnzeel et al., 2011). Collectively, these processes enable forest cover in this arid region, where annual net precipitation is much lower than the expected water demand of forest (Hildebrandt et al., 2007).

The cloud forest is crucial to ecosystem functions and services in the CSAM. For example, groundwater recharge rates have been found to be markedly higher (24%) in highly forested areas compared to sparsely forested areas (Friesen et al., 2018). Moreover, the cloud forest provides forage resources for pastoralism, and opportunities for tourism and recreation. The CSAM are part of the Horn of Africa biodiversity hotspot (Mittermeier et al., 2004), and support unique biodiversity assemblages, including the last viable population of critically endangered Arabian leopards (Spalton and Al Hikmani, 2014). However, decreasing long-term rainfall trends suggest the region is vulnerable to climate change (AlSarmi and Washington, 2011), and scientists have warned of the potential for irreversible forest-grassland regime shifts, due to reduced fog interception following removal of woody vegetation by browsing livestock (Hildebrandt and Eltahir, 2006, 2008).

In view of the high conservation and ecosystem service value of the cloud forest, improving our understanding of the ecohydrology in the CSAM is of great importance. While the density of the fog can be seen to vary in different parts of the mountains, no studies have examined how the complex topography affects fog distributions. In fact, our overall understanding of topography-fog interactions is limited; based on a small number of studies involving in situ measurements (Kidron, 2005; Hesse, 2012; Cavelier and Guillermo, 1989). Furthermore, we have a limited understanding of how fog distributions affect vegetation distributions at the landscape scale in the CSAM, with much of the previous ecohydrological

research having been conducted in a single forest plot. One exception is a recent study by Sousa *et al.* (2019), which provides evidence of a coupling between fog distributions and vegetation phenology. They concluded that vegetation phenology differed longitudinally, however it appears that their results were capturing the differing phenology of grasslands and forests, due to a misclassification of western and central forests as grasslands and eastern grasslands as forests.

Using conventional methods of fog detection (in-situ fog collectors, fog detectors and fog-droplet spectrometers) to conduct a detailed landscape-scale analysis of the interplay between topography, fog and vegetation would require an impractically large number of in-situ fog measurements (Bruijnzeel et al., 2005). Instead, several remote sensing approaches have been developed, although no satellites can detect fog specifically. The most common method involves differencing thermal (10.8 μm) and mid-infrared (3.7 μm) spectral bands. Fog is discriminated from other surfaces due to its low emissivity in mid-infrared at night and its high reflectivity during the day (Bendix, 2002). This method does not differentiate between fog and other cloud types, and is usually limited to night-time imagery. Another more recent method uses spectral, spatial and microphysical properties of fog from Meteosat 8 data (Cermak and Bendix, 2008). These methods have been used to describe fog-vegetation relationships, such as in Oman's central desert (Borrell et al., 2019) and elsewhere (Lehnert et al., 2018; Cereceda et al., 2008; Obregon et al., 2014; Cermak, 2012). However, one drawback of these methods is that fog distributions are mapped at a low resolution, of no less than 1.1 km (AVHRR imagery). To detect small or spatially heterogenous fog events higher resolutions are required, such as those of Landsat imagery (Bruijnzeel et al., 2005; Lehnert et al., 2018).

In this study, we develop a new high-resolution fog detection technique using Landsat data, and compile a suite of high-resolution geospatial datasets, to examine the interplay between topography, fog and vegetation in the CSAM. We address two research questions. Firstly,

how do topographic factors affect the distribution of monsoon fogs? And secondly, how do topographic factors and fog distributions affect patterns of vegetation greenness?

2. Materials and Methods

2.1. Topography and vegetation datasets

The geospatial datasets used in this analysis are listed in Table 1 and hosted in the PANGAEA data repository (doi.org/10.1594/PANGAEA.902295). The ArcGIS Spatial Analyst toolbox and the Geomorphometry and Gradient Metrics toolbox (Evans et al., 2014) were used to calculate a range of topographic layers and geomorphology metrics from ASTER Global Digital Elevation Model (GDEM) data. In addition, several layers were produced to account for topoclimatic phenomenon specific to the CSAM. The first was a binary layer to differentiate the north and south escarpments of the continental divide, which have contrasting climatic conditions. Without this variable, topographic variables such as elevation were torn between the two sides when predicting fog distributions. Surface aspect was derived from a low resolution (1 km) DEM to identify the continental divide. The second layer, a measure of fog exposure, was produced by reclassifying aspect to have highest values on slopes facing offshore in the direction of maximum fog exposure (an aspect of 160°) and lowest values on slopes facing inland (an aspect of 340°) (Abdul-Wahab, 2003). The third layer, a binary layer of fog exposure (windward/leeward), was calculated from the viewsheds of three observer points situated c. 60 km offshore at an elevation of 500 m.

Table 1. The geospatial datasets used in this analysis.

Metric	Description
Average monsoon fog density (0-1 scale)	A multiband (R, G, B, NIR) raster layer of average monsoon fog density calculated on a per cell basis as the mean of the fog reflectance values of 119 Landsat 5 TM scenes, 17 Landsat 7 ETM+ scenes and 121 Landsat 8 OLI TIRS scenes.
Fog temporal variability (0-1 scale)	A multiband (R, G, B, NIR) raster layer of fog temporal variability calculated on a per cell basis as the standard deviation of the fog reflectance values of 119 Landsat 5 TM scenes, 17 Landsat 7 ETM+ scenes and 121 Landsat 8 OLI TIRS scenes. This layer serves as a measure of temporal variability in fog density.

Normalized Difference Vegetation Index (NDVI) (Rouse et al., 1973)	An NDVI raster layer derived from Sentinel-2 imagery from April 2017. NDVI is a strong proxy of vegetation cover fraction, leaf area and biomass in arid environments.
Elevation	An elevation raster layer derived from ASTER Global Digital Elevation Map V2. The original data has been transformed to a projected coordinate system with bilinear resampling.
Slope (Burrough and Mcdonnell, 1998)	A raster layer of slope, in degrees, derived from the elevation layer using the average maximum technique.
Topographic Position Index (TPI) (Guisan et al., 1999). Nine layers with radii of 100 m, 200 m, 300 m, 400 m, 500 m, 1000 m, 2000 m, 3000 m, 5000 m, and 10000 m.	TPI raster layers using different radii derived from the elevation layer. TPI measures the difference between a central cell elevation and the average elevation around it within a predetermined radius (R). It is a measure of terrain roughness. TPI is increasingly used to classify slope position and landform types.
Linear Aspect	A linear aspect raster layer derived from the elevation layer. Circular aspect is transformed to a linear variable.
Terrain Ruggedness Index (TRI) (Riley et al., 1999)	A TRI raster layer derived from the elevation layer, based on the sum change in elevation between a central cell and its eight neighbouring cells. TRI is a terrain roughness metric.
Surface Area Ratio (SAR) (Berry, 2002)	A SAR raster layer derived from the elevation layer. SAR is another measure of terrain roughness which compares terrain surface area to the planimetric area. Berry's method uses slope to calculate an adjustment factor for the cell planimetric area.
Surface Relief Ratio (SRR) (Pike and Wilson, 1971)	A SRR raster layer derived from the elevation layer which describes terrain roughness using a central cell and its eight neighbouring cells.
Curvature (Moore et al., 1991)	A layer of curvature derived from the elevation layer. It is the second derivative value of the input surface on a cell-by-cell basis and describes the concavity or convexity of a surface.
Compound Topographic Index (CTI) (Gessler et al., 1995)	A CTI raster layer derived from the elevation layer. CTI is a steady state wetness index and a measure of flow accumulation. Higher values represent drainage depressions, while lower values represent hilltops and ridges.
Site Exposure Index (Balice et al., 2000)	A SEI raster layer derived from the elevation layer. SEI rescales aspect with higher values on warm south facing slopes and lower values on north facing slopes.
Topographic Radiation Aspect Index (TRASP) (Roberts and Cooper, 1989)	A TRASP derived from the elevation layer which assigns lowest values to cool, north-facing slopes and highest values to hotter, dryer south-facing slopes.
Escarpment (North/South)	A binary raster layer to differentiate the north and south watersheds of the continental divide. Produced by calculating aspect on a low resolution (1 km) DEM to identify the continental divide.
Modified aspect	A raster layer of reclassified aspect with highest values on slopes facing offshore in the direction of maximum fog exposure (an aspect of 160°) and lowest values on slopes facing inland (an aspect of 340°) (Abdul-Wahab, 2003).
Topographic exposure to fog	A binary raster layer of topographic exposure to monsoon fog (exposed/leeward). Calculated from the viewsheds of three observer points situated c. 60 km offshore at an elevation of 500 m.

Vegetation indices are combinations of two or more spectral bands which detect vegetation properties such as photosynthetic activity. The most commonly used is the normalized difference vegetation index (NDVI) (Rouse et al., 1974). In arid environments, NDVI is a strong proxy of vegetation cover fraction, leaf area and biomass (Tian et al., 2019). We derived NDVI from Sentinel-2 MSI data products. The Sentinel 2 Level 1C top-of-atmosphere reflectance data products were processed to Level 2A bottom-of-atmosphere data products using the Sen2Cor processer in the Sentinel 2 Toolbox in the Sentinel Application Platform (SNAP) (Zuhlke et al., 2015). Imagery from April 2017 was chosen because in April the distinction between habitat types is most pronounced. Trees and shrubs undergo a second generative growth phase (which was particularly pronounced in 2017 due to a strong monsoon the previous summer) while herbaceous species have senesced (Miller et al., 1988). A visual comparison of NDVI values with satellite imagery shows that high NDVI values correspond to cloud forest, lower values correspond to grasslands, and the lowest values indicate unvegetated areas.

2.2. Fog density dataset

Satellite observations show some consistency in the monsoon fog distributions in the CSAM. For example, some areas of the mountains receive frequent dense fogs, while other areas receive infrequent fogs. We hypothesized that topographic factors influence the fog distribution, which interacts with the land surface and influences vegetation distributions. Therefore, we produced a raster layer of average monsoon fog density, calculated on a per cell basis as the mean of the fog reflectance values of multiple Landsat scenes. In addition, we calculated a layer of standard deviation values, as a measure of fog temporal variability.

These layers were calculated in Google Earth Engine (see Supplement 1 for JavaScript code). First, the Landsat 5, 7 and 8 top-of-atmosphere reflectance imagery collections were filtered to imagery from the CSAM acquired during the monsoon (June-September). Then, scenes with no or very little fog, or a high coverage of mid-level or high-level clouds, were filtered out. This was achieved by filtering out scenes with less than 5% cloud cover (using Google

Earth Engine's pixel-based cloud scoring algorithm) over the fog-affected southern escarpments or more than 5% cloud cover to the north of the mountains (Figure 2). This technique successfully filtered out cloudy scenes because the monsoon fog is restricted to the vegetated southern escarpments, and thus substantial areas of cloud outside this typical distribution, is very likely to be mid-level and high-level clouds, rather than fog.

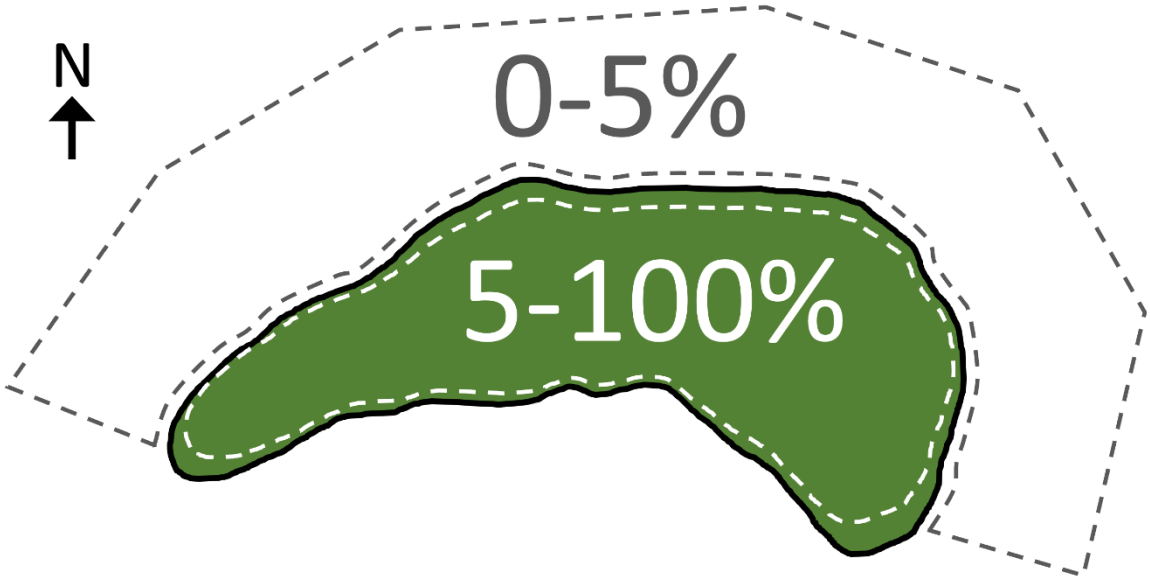

Figure 2. A diagram illustrating the criteria employed for filtering out scenes with little or no fog (< 5% over the mountains) or a high coverage of mid-level or high-level clouds (> 5% to the north of the mountains) prior to calculating the average fog density. One hundred and nineteen of 251 Landsat 5 scenes, 17 of 36 Landsat 7 scenes and 121 of 232 Landsat 8 scenes remained after removing fogless and cloudy scenes.

The scenes were cropped to remove ragged edges or bordering 'no data' values, to ensure a seamless final composite layer. Then, the fog cover was extracted from each scene using the cloud bitmask (4) in the quality assessment band (BQA), and the background cells were set to zero to represent fogless areas (a reflectance threshold could also have been used to select fog areas). This extraction method, using a cloud bitmask, was effective because the monsoon fog in the CSAM is dense and contrasts with the land surface. Thus, it should be

noted that this method may not be appropriate for isolating low density or irregular fog events, or distinguishing between fog, haze and low stratus.

Fog reflects solar radiation in the visible and infrared spectra (Wang et al., 1999). In the CSAM, higher reflectance values in fog areas can be interpreted as denser and more moisture-laden fog because the fogs lower and upper altitudes are limited by the southern escarpment and a temperature inversion, respectively (Kürschner et al., 2004; Friesen et al., 2018). A histogram of the band reflectance values confirmed the green, red, blue and near-infrared (NIR) bands detected the greatest range of fog reflectance values (Figure 3). These bands were isolated in each image and renamed for continuity between sensors.

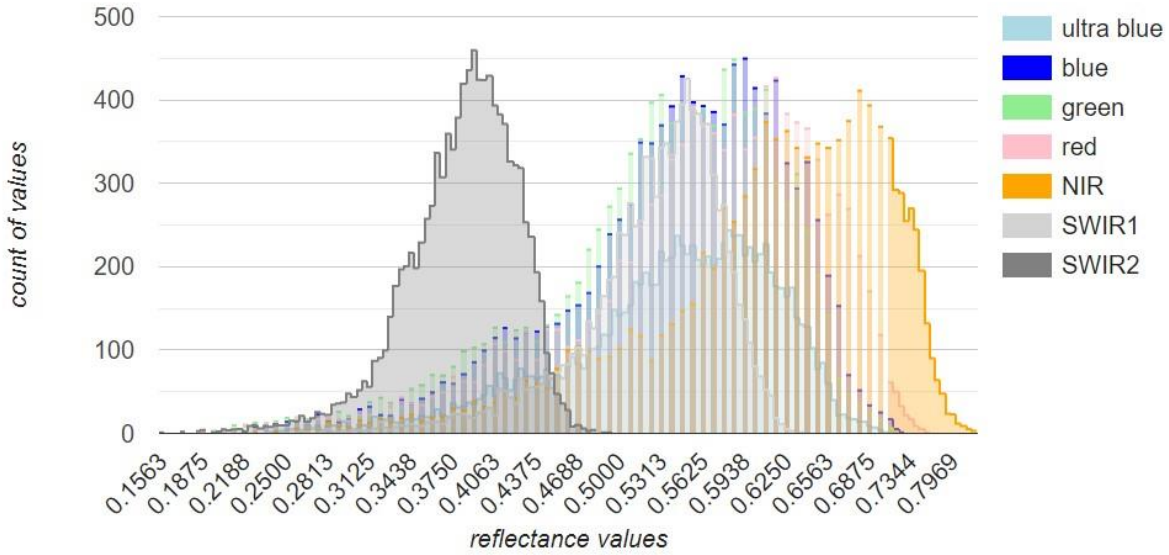

Figure 3. Histograms of the band reflectance values in fog areas. The NIR band detects the greatest range of reflectance values in fog areas, and thus the range of fog densities are well-represented.

A total of 257 scenes acquired in the years 1987–2002 and 2013–2019 were included in the mean and standard deviation calculations (Supplement 2). The number of scenes and their locations (WRS-2 path/row) in each represented monsoon season, are shown in Figure 4, along with their fog intensity. Fog intensity was calculated for each scene as the mean of the

fog density cell values within an analysis window. Each tile area (WRS-2 path/row) contained an analysis window, within which every scene had complete data.

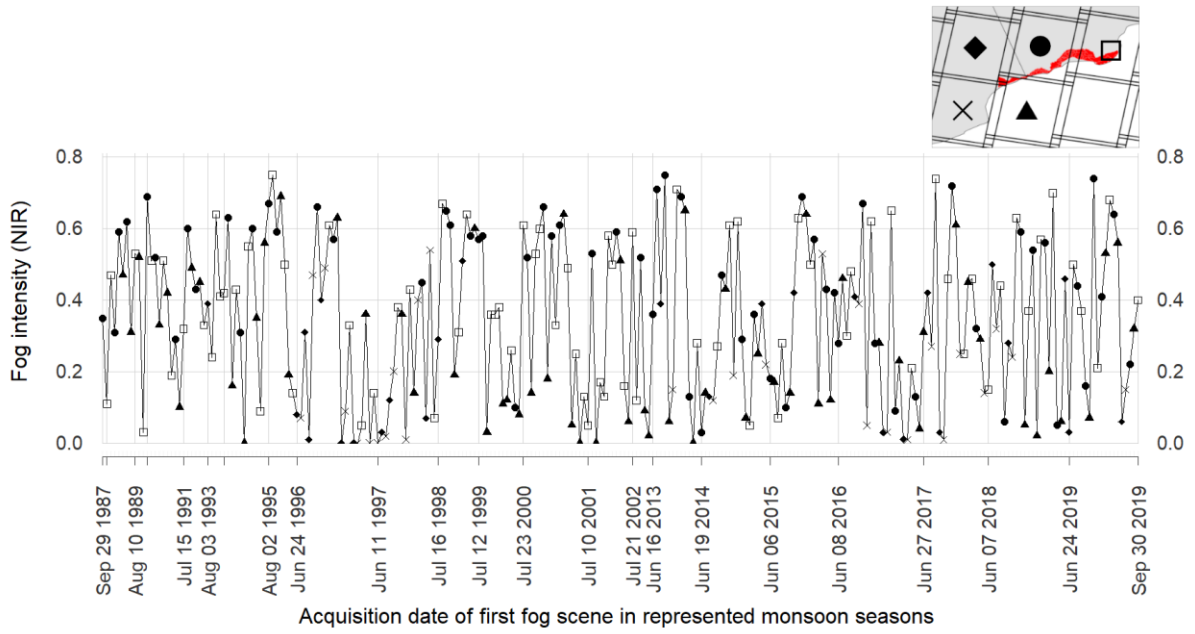

Figure 4. The number of scenes (total 257) and their locations (WRS-2 path/row) in each represented monsoon season (1987-2002 and 2013-2019). Fog intensity was calculated for each scene as the mean of the fog density cell values within an analysis window. Each tile area (WRS-2 path/row) contained an analysis window, within which every scene had complete data.

Finally, the scenes were stacked, and the mean and standard deviation were calculated on a per cell basis, to produce layers of average fog density and fog temporal variability, respectively. The NIR band was used in this analysis as it detects the greatest range of reflectance values in fog areas, and thus the range of fog densities are well-represented (Figure 3).

To confirm that the fog density layer was spatially accurate and interacting with the land surface and affecting vegetation patterns, we used data from a 2016 botanical survey of the cloud forest in the Jabal Qamar mountain range in Dhofar (Ball, 2019). The original dataset comprised 7200 woody plant records from 30 systematically sampled sites between 300 m

and 900 m above sea level (Figure 1). To validate the fog layer, an ANOVA test was used to compare fog density values at the locations of four xerophytic plant species (*Acacia gerrardii*, *Adenium obesum*, *Aloe praetermissa* and *Cordia ovalis*) with fog density values at the locations of four relatively mesophytic plant species (*Blepharis dhofarensis*, *Cordia perrottetii*, *Croton confertus* and *Ruttya fruticosa*).

2.3. Testing the topography-fog-vegetation relationship

To produce a testable dataset the geospatial layers were randomly sampled at 50,000 locations throughout the monsoon area of the CSAM (fog density > 0.1). We excluded the city of Salalah on the coastal plain and areas within 50 m of surfaced roads, to avoid sampling terrain disturbance and anthropogenic features. The sample was analysed using regression tree analysis (RTA) in the R 'rpart' package (R Core team, 2019; Therneau and Atkinson, 2019b) which implements methodologies of Breiman *et al.* (1984). Two trees were grown. The first tree modelled fog density as a function of topographic variables and included 22 explanatory variables (Table 1). The second tree modelled vegetation greenness as a function of fog and topographic variables, using the same 22 topographic variables, plus fog density and fog temporal variability.

Regression tree analysis partitions a dataset into smaller subgroups through recursive partitioning. The binary splits occur at nodes based on true/false answers about the values of predictors, and each split is based on a single variable. The rule generated at each step maximizes the class purity within each of the two resulting subgroups (Breiman et al., 1984; Miska and Jan, 2004). It is a popular alternative to classical regression techniques with several characteristics that make it well-suited to our analysis. Firstly, it is a non-parametric technique which befits the heteroscedasticity and non-normality of our response variables. Secondly, it does not rely on a priori hypotheses about the relationships between the predictors and the response variable. This is important in geomorphological and remote sensing analyses where nonlinear responses and predictors may interact in unknown ways (Miska and Jan, 2004). Finally, RTA accepts both categorical and continuous predictors and

models interaction effects, and represents them in a highly interpretable format (Thuiller et al., 2003).

Deciding on the appropriate length of the tree is a key consideration in RTA. If the tree is too short (underfitting) it could have a high predictive error and underexplain the data, but if it is too long (overfitting) it will describe random 'noise' in the data and become complex and uninterpretable (Spruill, Showers and Howe, 2010; Therneau and Atkinson, 2019a). The rpart package performs cross-validations to determine an appropriate complexity parameter for tree pruning. Between 10 and 20 cross-validations are recommended, so 15 cross-validations were chosen. Any split that does not decrease the overall lack of fit by a factor of the complexity parameter at each step is not attempted (Prasad et al., 2006). By default, the rpart package implements a minimum complexity parameter of 0.01, but Therneau and Atkinson (2019a) warn of underfitting with large datasets. For our tree which modelled vegetation greenness, we reduced the complexity parameter to 0.005, which increased the number of terminal nodes from eight to ten. Variable importance was calculated using the default method in the rpart package from Breiman *et al.* (1984), as the sum of the goodness of split measures (Gini index) for each variable used as a primary or surrogate split. The minimum number of observations required for a split and for a terminal node was specified as 20.

3. Results

The fog density and fog temporal variability layers are displayed in Figure 5, alongside a true-colour satellite image, NDVI, and elevation. Visually, broadscale correlative patterns are evident. In Figure 6, fog density is plotted against fog temporal variability, which shows a curvilinear relationship, with increasing temporal fog variability until a fog density of 0.4, and then decreasing fog variability with increasing fog density. Fog data at the locations of the eight moisture-sensitive plant species are also plotted in Figure 6, and an ANOVA test confirmed that fog densities are significantly higher in areas occupied by the mesophytic species ($F(1, 94) = 65.7$, $p = < 0.001$). This indicates that our fog detection method is

accurate and that the observed fog distribution is interacting with the land surface and affecting vegetation patterns. Figure 7 shows a detailed cross-section of the CSAM with the layer of fog density draped over a double-exaggerated, contoured, shaded relief elevation surface.

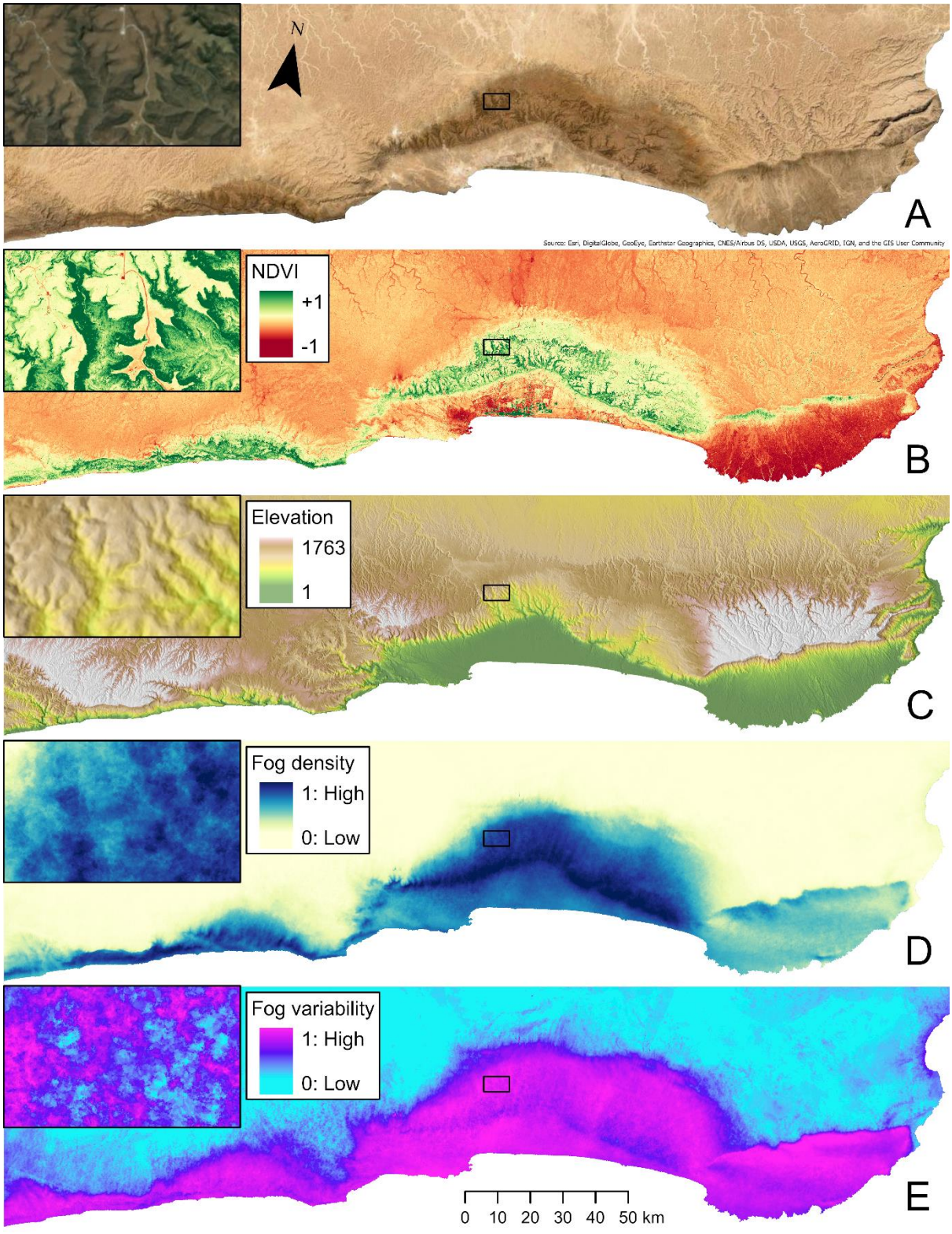

Figure 5. Layers of (a) true-colour satellite image, (b) NDVI, (c) elevation, (d) average fog density, and (e) fog temporal variability, for the central South Arabian mountains. Broadscale correlative patterns are evident. Diffference in NDVI between cloud forest and grassland can be seen in the inset maps.

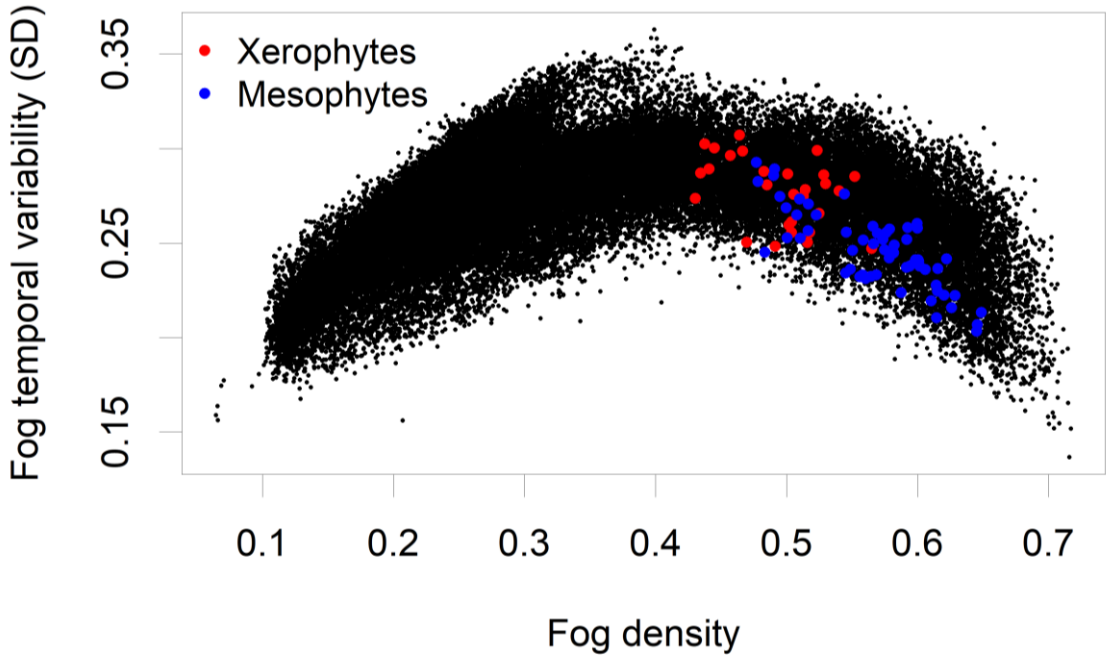

Figure 6. A scatterplot of fog density and fog temporal variability. The curvilinear relationship shows increasing and high temporal fog variability in areas with low fog densities (< 0.4) but lower and decreasing fog variability in areas of high fog densities. Fog density is significantly higher ($p < 0.001$) and temporal variability lower for mesophytes compared to xerophytes, providing evidence that the fog density layer is accurate.

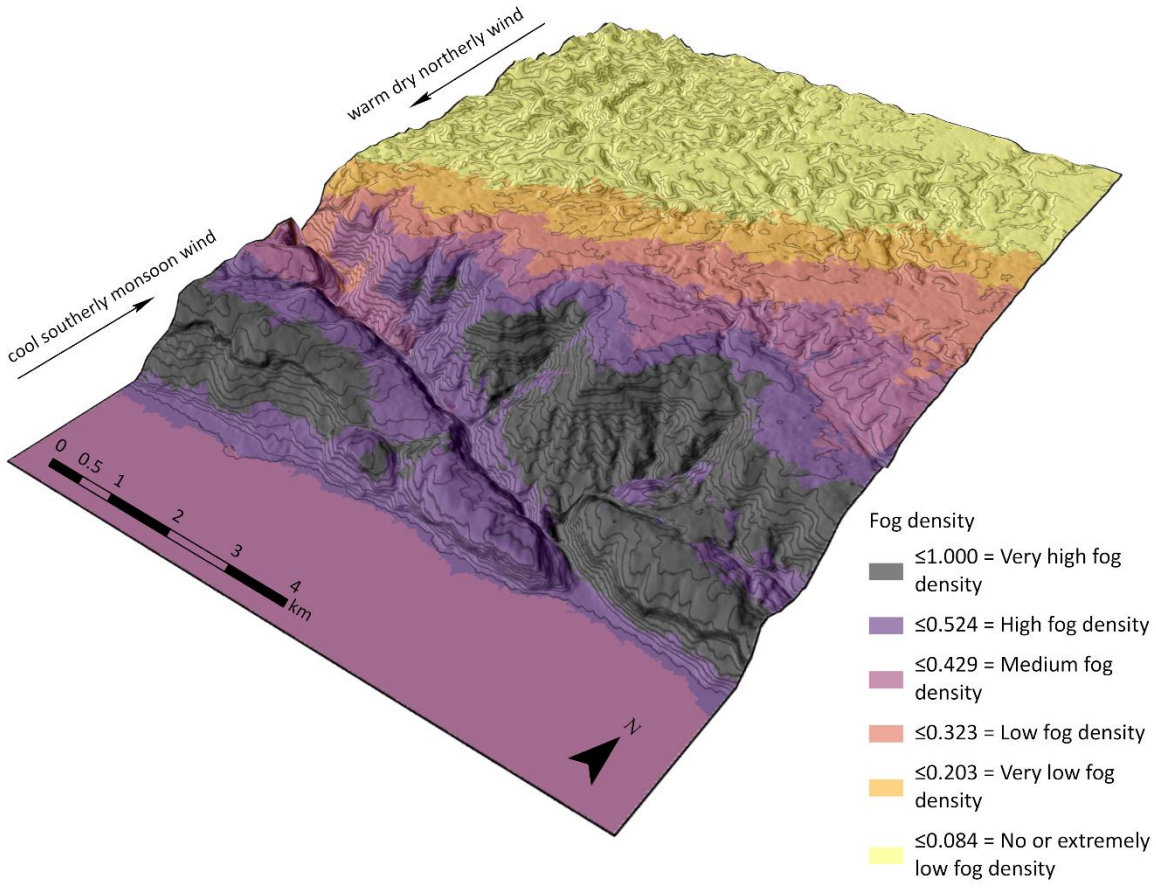

Figure 7. A three-dimensional cross section of the central South Arabian mountains between Dhalkut and Rakhyut in Dhofar, with the layer of fog density draped over a double-exaggerated, contoured, shaded relief elevation surface. Fog density has been classified into six classes (Jenks optimization). Steep windward slopes obstruct the inland movement of fog affecting its distribution.

In the following section we present the RTA trees (Figure 8 and 9) and diagnostic plots (Figure 10). The complexity parameter plots show the reduction in the cross validated error with decreasing complexity parameter values and increasing tree size (Figure 10). They show that we would see diminishing returns if we continued to grow the trees. Additional plots show the importance of each variable (Figure 10). The higher the variable importance (0-1 range), the more the variable contributes to improving the model.

The tree to describe fog distributions had 10 splits, 11 terminal nodes and a cross-validated error of 0.582 (Figure 8, Supplement 3). The most important variables (importance > 0.05) are shown in Figure 10.

In RTA, partitions near the starting node are the most important and result in large reductions in model error. At the first split, the tree identified an important elevation threshold at 858 m. This represents the boundary of the core fog zone, where the southern escarpments meet the plateau, where an atmospheric temperature inversion limits the northward movement of fog (Kürschner et al., 2004; Friesen et al., 2018). The lowest fog densities occurred at elevations above 1027 m (Node 4) and on the northern desert-facing escarpments (Node 14). On the southern escarpments, low fog densities occurred in leeward areas above 858 m (Node 10) and on hilltops below 300 m (Node 12). The topographic position index (TPI) describes whether land is within wadis and depressions or on crests and hilltops. Higher fog densities occurred in wadis between 300 m and 858 m (Node 30), on leeward-facing wadi slopes below 300 m (Node 26), and on windward-facing slopes between 858 m and 1027 m (Node 11). Higher fog densities occurred on hilltops in leeward areas between 300 m and 858 m (Node 124), where fog densities were markedly higher on steep slopes (Node 125), as measured by Surface Area Ratio. High fog densities occurred on windward wadi slopes below 300 m (Node 27), with the highest on windward hilltops between 300 m and 858 m (Node 63). In summary, fog densities are low above 858 m unless in windward areas, whilst below 858 m, higher fog densities occur in wadis at lower elevations and on hilltops at higher elevations. At all elevations, fog densities are higher in windward locations.

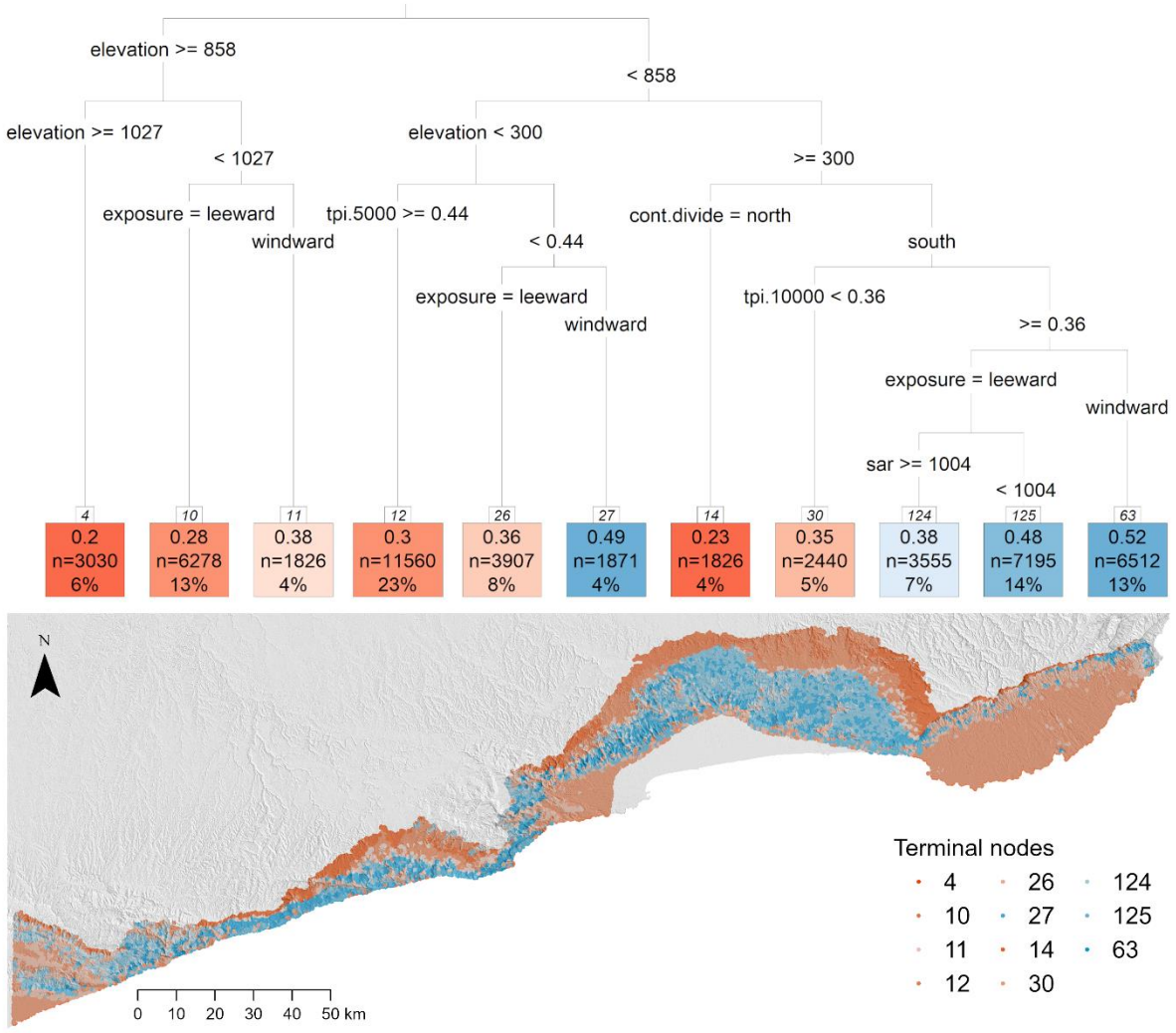

Figure 8. The tree describing fog distributions had 10 splits, 11 terminal nodes and a cross-validated error of 0.582. The 'jumps' in the node numbers result from the pruning of those branches which did not decrease the overall lack of fit by a factor of complexity parameter. The terminal node numbers were reassigned to the data points and mapped according to the tree colour scheme.

The tree describing vegetation distributions had 9 splits, 10 terminal nodes and a cross-validated error of 0.349 (Figure 9, Supplement 4). The most important variables (importance > 0.05) are shown in Figure 10.

The first partition at a fog density threshold of 0.37 reduced the cross-validated error from 1 to 0.6, indicating the importance of this first split which represents the boundary of the core fog zone. Low NDVI values were found to be in areas with fog densities below 0.37, with the

lowest at elevations below 293 meters. Here, NDVI values were lower on hilltops (Node 8) than in wadis (Node 9). Slightly higher NDVI values occurred at elevations above 293 m in areas with fog densities below 0.29 (Node 10), in areas with smooth terrain below 164 m with fog densities above 0.37 (Node 12), and in areas above 293 m with fog densities between 0.29 and 0.37 (Node 11). Higher NDVI values were on hilltops with smooth terrain (Terrain Ruggedness Index) above 164 m, in areas with fog densities greater than 0.37 (Node 26), and in areas with rougher terrain with fog densities between 0.37 and 0.44 (Node 14). Higher NDVI values occurred in areas with rugged terrain and fog densities greater than 0.44 (Node 30) and in wadis with smooth terrain above 164 m and fog densities greater than 0.37 (Node 27). The highest NDVI values occurred in areas with very rugged terrain and fog densities greater than 0.44 (Node 31). In summary, the lowest NDVI values occurred in areas with fog densities below 0.37 and at low elevations (< 164 m), whilst higher NDVI values were in foggier areas, especially within wadis and areas with rugged terrain.

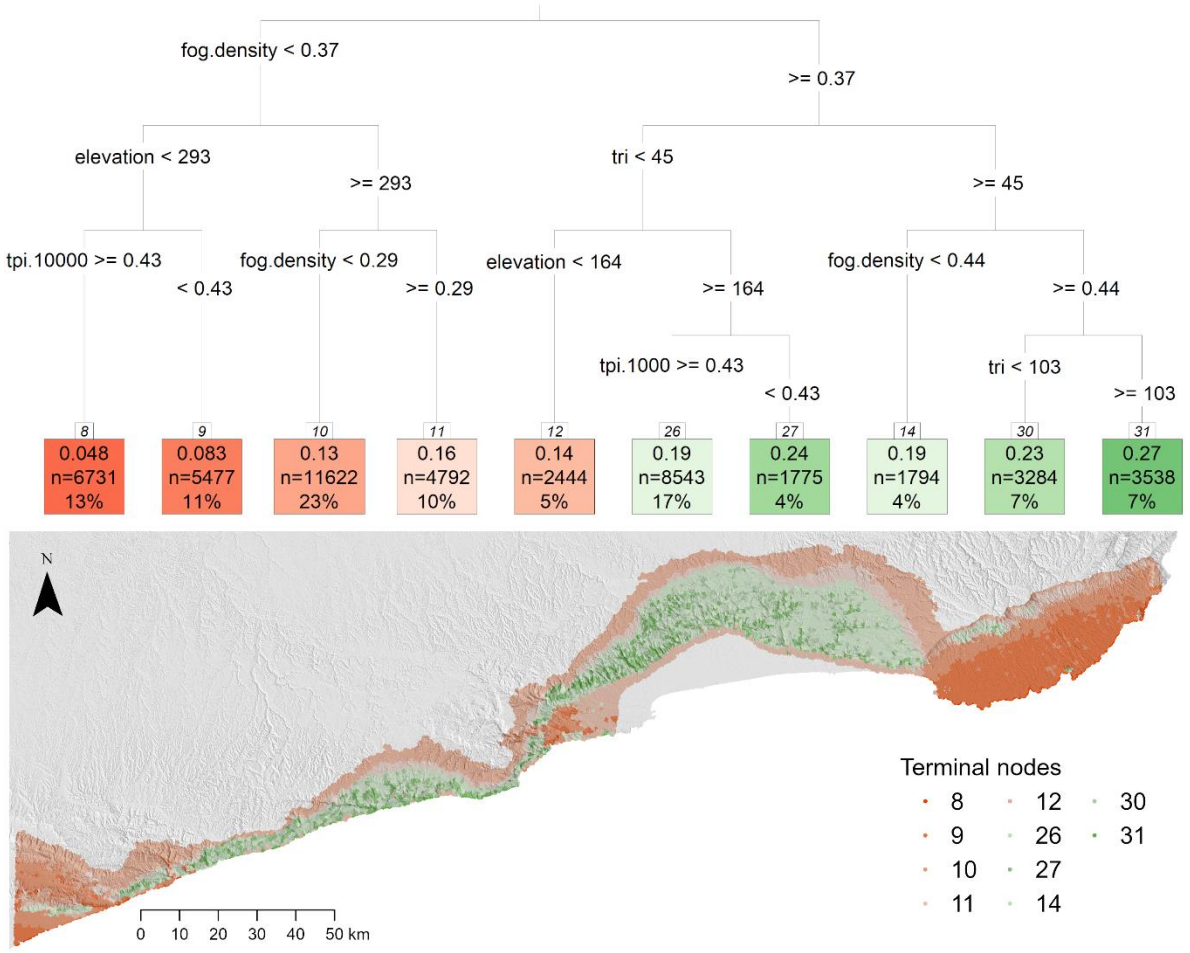

Figure 9. The tree describing vegetation distributions had 9 splits, 10 terminal nodes and a cross-validated error of 0.349. The 'jumps' in the node numbers result from the pruning of those branches which did not decrease the overall lack of fit by a factor of complexity parameter. The terminal node numbers were reassigned to the data points and mapped according to the tree colour scheme.

To further test the importance of fog, relative to topographic variables, for describing vegetation distributions (in addition to the variable importance results in Figure 10), we ran the analysis of vegetation greenness distributions without fog data. Less variance was explained - elevation was the most important variable (0.44), but a cross-validated error of only 0.56 was reached by the ninth split, compared to 0.35 with fog data included.

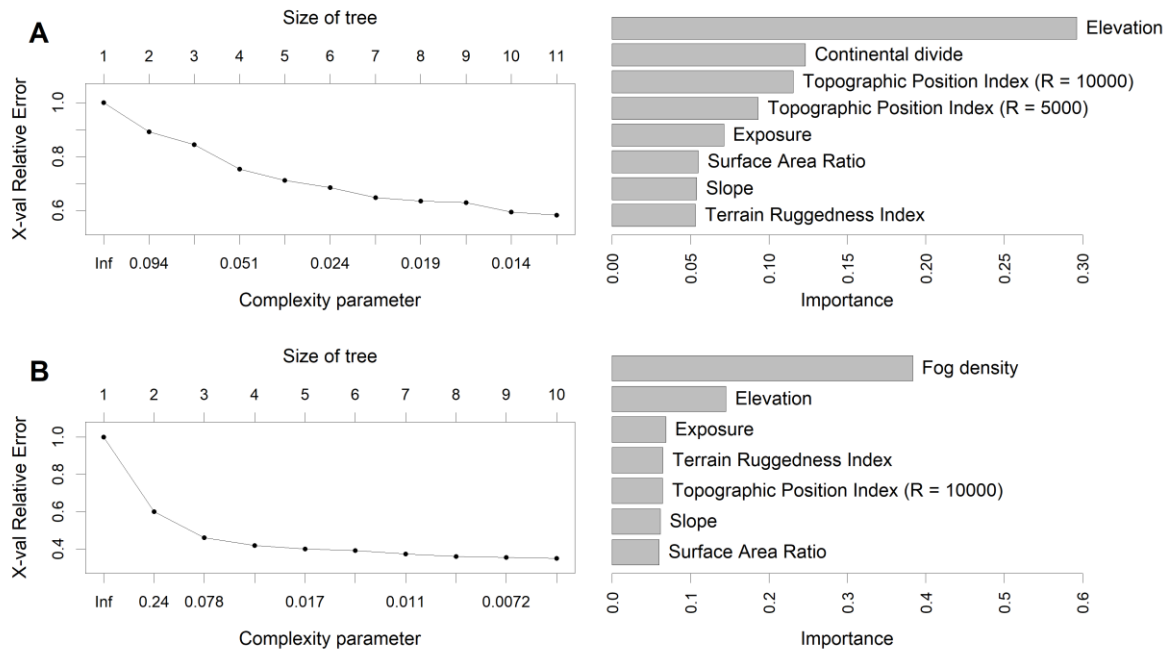

Figure 10. Complexity parameter plots and variable importance for (a) the tree describing fog distributions and (b) the tree describing vegetation distributions. Complexity parameter plots show the reduction in the cross validated error with decreasing complexity parameter and increasing tree size. We would see diminishing returns if we continued to grow the trees. Variable importance is calculated as the sum of the goodness of split measures (Gini index) and considers both primary and surrogate splits.

4. Discussion

The first tree in our analysis described 42% of the variance in fog distributions, showing that topographic factors play a substantial role in shaping fog distributions. Altitudinal variation in fog distributions was identified, with important thresholds at 858 m and 1027 m, which correspond to the boundary of the core fog zone and fog spillover to the northern escarpments, respectively (Figure 8). Topographic position and exposure were important (Figure 10). Our results show that at low elevations fog density is higher in wadis than on hilltops, whilst at higher elevations fog density is lower in wadis (Figure 8). One explanation for this pattern is that at lower elevations, wadis are larger and deeper and oriented with their mouths in a windward direction, and therefore can collect fog. However, at higher elevations the wadis are shallower and oriented in various directions, and therefore the fog passes over them, assisted by the higher wind speeds at altitude.

Regarding exposure, we see high fog densities where windward slopes and landforms, such as cliffs, obstruct the inland movement of fog, whilst lower fog densities occur in leeward locations (Figure 7). Lawton (1978) described a similar trend from Dhofar but at a much smaller scale. Moisture-deprived shadows of bare ground on the lee-side of *Euphorbia balsamifera* shrubs were noted. Our results, which show the greatest fog densities on steep windward slopes, conform to findings from other studies which used in-situ field measurements. For example, windward aspects received higher fog precipitation than leeward aspects in the Negev desert (Kidron, 2005) and fog densities were found to be lower in leeward locations in coastal Peru (Hesse, 2012). Furthermore, over twice as much fog was intercepted by forests on exposed windward slopes than on leeward slopes in Columbia and Venezuela (Cavelier and Guillermo, 1989).

The second tree in our analysis described considerable variance in vegetation greenness (65%) and fog density was the most important predictor (Figure 9). Fog is known to influence vegetation patterns (Scholte and De Geest, 2010; Martorell and Ezcurra, 2002; Cavelier and Guillermo, 1989), especially in arid environments (Hildebrandt and Eltahir,

2008; Scholte and De Geest, 2010; Martorell and Ezcurra, 2002). Our results corroborate existing evidence of the importance of fog for vegetation communities in the CSAM (Hildebrandt et al., 2007; Hildebrandt and Eltahir, 2007).

Our results also show that vegetation greenness increases with fog density. In areas with the highest and most consistent fog densities we see the highest NDVI values (Figure 9). In these locations, fog interception by the cloud forest increases soil moisture availability, therefore sustaining its own ecological niche (Hildebrandt et al., 2007; Hildebrandt and Eltahir, 2006). Interestingly, our results show that these areas also have high terrain roughness (Figure 9), which presumably gives rise to a complex forest canopy structure, which is known to intercept more fog moisture than a continuous, smooth canopy (Hildebrandt and Eltahir, 2008). Therefore, these areas, such as at the base of cliffs or tops of tributaries, represent important hotspots of fog interception.

Several of our findings provide evidence that regional vegetation patterns more closely follow a fog, rather than an altitudinal gradient, as conventionally supposed (Patzelt, 2015; Mosti et al., 2012; Raffaelli and Tardelli, 2006). Firstly, our results show that fog density and vegetation greenness vary at comparable altitudes. Secondly, the variable importance data shows that topographic factors such as exposure and topographic position are collectively as important as elevation in describing fog distributions (Figure 10). Finally, fog density was much more important than elevation in describing vegetation greenness (Figure 10). Indeed, much less variance was explained when we ran our analysis of vegetation greenness distributions without fog data. An altitudinal gradient in fog moisture may also be suppressed in the CSAM due to the counteracting effects of elevation and distance from the coast. Generally, coastal advection fog interception increases with altitude within the fogs elevation range, due to concurrent increases in fog frequency (immersion time) and wind speed (Bruijnzeel et al., 2005). However, fog interception tends to decrease with distance from the coast (Cereceda et al., 2002).

The layer of fog density describes patterns of vegetation greenness more accurately than topographic factors alone, perhaps as it incorporates unmeasured topoclimatic processes. Therefore, the layer of fog density represents an important variable for ecological modelling of biodiversity in the region, especially for plants which respond strongly to moisture availability. In recent years, the number of botanical records from the CSAM has increased substantially, thanks to the efforts of the Oman Botanic Garden (Patzelt et al., 2008, 2009). Besides plants, specialist animal species (many of which have received very little research attention), are also likely to respond to fog density. For example, humidity has been cited as an important factor in the ecological separation of species of *Hemidactylus* geckos in Dhofar (Carranza and Arnold, 2012), whilst different bird communities have been described from habitats with different water availability in western Dhofar (Ball et al., 2015). It should also be noted that by advancing our ability to model abiotic conditions, we improve our ability to quantify the relative effects of human disturbances on vegetation patterns in the CSAM, which will be one focus of our future research.

This research contributes a novel, high-resolution, fog detection technique which is particularly suited to mapping dense fog events with complex spatial distributions. However, there are two main limitations to our fog detection technique. Firstly, it may not be appropriate for detecting low density or irregular fog events, or distinguishing between fog, haze and low stratus. The fog needs to contrast with the land surface to be extracted using a cloud mask or reflectance threshold, and to minimise the influence of land surface reflectance values on fog reflectance values. Secondly, the measures of fog density are unitless. Thus, comparisons with other studies is difficult, unless liquid water content values from multiple field measurements are interpolated in the fog density layer.

There are also two main limitations to our analysis. Firstly, we cannot determine if the fog layer is touching the local surface or not. Thus, ground fog and raised fog are lumped together. This is common to other remote sensing fog detection methods. However, our results show beyond reasonable doubt that our observed fog distributions are affecting

vegetation processes. Secondly, other unmeasured thermodynamic processes, such as cold air pooling (Hang et al., 2016), turbulence (Gultepe et al., 2007), wind (Walmsley et al., 1996) or changes in the frequency, depth, and strength of atmospheric inversions (Abdul-Wahab, 2003), will influence fog distributions. These may account for some of the cross-validated error (0.582) in the tree describing fog distributions, in addition to variability associated with the landscape scale of the analysis.

Conclusion

In the central South Arabian mountains of Yemen and Oman, fog interception by the vegetation supports ecosystem functions and services. Yet we have a limited understanding of the factors affecting fog distributions and their cumulative effects on vegetation. In this paper, we developed a novel method of high-resolution fog detection using Landsat data and assembled a suite of geospatial datasets. Regression tree analysis was then used to examine the topographic factors influencing fog distributions and the topoclimatic factors influencing satellite-derived vegetation greenness. We found that topography affects fog distributions. Specifically, steep windward slopes obstruct the inland movement of fog, resulting in heterogenous fog densities and hotspots of fog interception. Moreover, we found a positive spatial trend between fog density and vegetation greenness. In addition, we found that the layer of fog density describes vegetation patterns more precisely than topographic factors alone, and we propose that the average fog distribution, rather than an elevation gradient, may be more appropriate to describe regional vegetation patterns. The layer of fog density will enable an improved understanding of how local biodiversity, much of which is endemic, range-restricted, or in decline, responds to local variability in topoclimatic conditions.

Acknowledgements: This work was supported by the UK Economic and Social Research Council [award reference 1595870] and the US National Science Foundation [grant number 1617185].

Data accessibility: The geospatial datasets used in this analysis are hosted in the PANGAEA data repository (doi.org/10.1594/PANGAEA.902295) and the botanical survey data is hosted in the Mendeley data repository (doi.org/10.17632/dc97zn6gzc.1)

Literature cited

Abdul-Wahab, S.A. 2003. Analysis of thermal inversions in the Khareef Salalah region in the Sultanate of Oman. *J. Geophys. Res.* **108**, 1–8. https://10.1029/2002JD003083.

AlSarmi, S., and R. Washington. 2011. Recent observed climate change over the Arabian Peninsula. *J. Geophys. Res. Atmos.* **116**, 1–15. https://10.1029/2010JD015459.

Balice, R.G., J.D. Miller, B.. Oswald, C. Edminister, and S.R. Yool. 2000. Forest surveys and wildfire assessment in the Los Alamos; 1998–1999. Los Alamos National Laboratory, University of California, Los Alamos. pp. 93.

Ball, L. 2019. Data from a botanical survey of the Anogeissus cloud forest in Jabal Qamar, Dhofar, Oman. *Mendeley Data*. **V1**. https://http://dx.doi.org/10.17632/dc97zn6gzc.1#file-f2b43852-d06e-459e-8716-e08834c4d0e4.

Ball, L., W. Al Fazari, and J. Borrell. 2015. Birds of Wadi Sayq, Dhofar, Oman: British Exploring Society expeditions January–March 2012 and 2013. *Sandgrouse*. **37**, 2–12.

Bendix, J. 2002. A satellite-based climatology of fog and low-level stratus in Germany and adjacent areas. *Atmos. Res.* **64**, 3–18. https://10.1016/S0169-8095(02)00075-3.

Berry, J.K. 2002. Use surface area for realistic calculations. *Geoworld*. **15**, 20–21.

Borrell, J.S., G. Al Issaey, D.A. Lupton, T. Starnes, A. Al Hinai, S. Al Hatmi, R.A. Senior, T. Wilkinson, J.L.H. Milborrow, A. Stokes-rees, and A. Patzelt. 2019. Islands in the desert: environmental distribution modelling of endemic flora reveals the extent of Pleistocene tropical relict vegetation in southern Arabia. *Ann. Bot.* **mcz085**, 1–12. https://10.1093/aob/mcz134.

Breiman, L., J.H. Friedman, R.A. Olshen, and C.J. Stone. 1984. Classification and regression trees. Taylor & Francis, Monterey. pp. 368.

Bruijnzeel, L.A., M. Mulligan, and F.N. Scatena. 2011. Hydrometeorology of tropical

montane cloud forests: emerging patterns. *Hydrol. Process.* **25**, 465–498. https://10.1002/hyp.7974.

Bruijnzeel, L.S., W. Eugster, and R. Burkard. 2005. Fog as a Hydrologic Input. *In* Encyclopedia of Hydrological Sciences. John Wiley & Sons, New York.

Burrough, P.A., and R.A. Mcdonnell. 1998. Principles of Geographical Information Systems. Oxford University Press, Oxford. pp. 333.

Carranza, S., and E.N. Arnold. 2012. A review of the geckos of the genus Hemidactylus (Squamata: Gekkonidae) from Oman based on morphology, mitochondrial and nuclear data, with descriptions of eight new species. *Zootaxa*. **3378**, 1–95.

Cavelier, J., and G. Guillermo. 1989. Mist and fog interception in elfin cloud forests in Colombia and Venezuela. *J. Trop. Ecol.* **5**, 309–322.

Cereceda, P., H. Larrain, P. Osses, M. Farías, and I. Egaña. 2008. The spatial and temporal variability of fog and its relation to fog oases in the Atacama Desert, Chile. *Atmos. Res.* **87**, 312–323. https://10.1016/j.atmosres.2007.11.012.

Cereceda, P., P. Osses, H. Larrain, M. Farías, M. Lagos, R. Pinto, and R.S. Schemenauer. 2002. Advective, orographic and radiation fog in the Tarapacá region, Chile. *Atmos. Res.* **64**, 261–271. https://10.1016/S0169-8095(02)00097-2.

Cermak, J. 2012. Low clouds and fog along the South-Western African coast - Satellite-based retrieval and spatial patterns. *Atmos. Res.* **116**, 15–21. https://10.1016/j.atmosres.2011.02.012.

Cermak, J., and J. Bendix. 2008. A novel approach to fog/low stratus detection using Meteosat 8 data. *Atmos. Res.* **87**, 279–292. https://10.1016/j.atmosres.2007.11.009.

Evans, J.S., J. Oakleaf, S.A. Cushman, and D. Theobald. 2014. An ArcGIS Toolbox for Surface Gradient and Geomorphometric Modeling, version 2.0-0. The Nature Conservancy and University of Wyoming, Laramie.

Friesen, J., M. Zink, A. Bawain, and T. Müller. 2018. Hydrometeorology of the Dhofar cloud forest and its implications for groundwater recharge. *J. Hydrol. Reg. Stud.* **16**, 54–66. https://10.1016/j.ejrh.2018.03.002.

Gessler, P.E., I.D. Moore, N.J. McKensie, and P.J. Ryan. 1995. Soil-landscape modelling and spatial prediction of soil attributes. *Int. J. Geogr. Inf. Syst.* **9**, 421–432. https://http://dx.doi.org/10.1080/02693799508902047.

Ghazanfar, S.A., and M. Fisher. 1998. Vegetation of the Arabian Peninsula. Kluwer Academic Publishers, Dordrecht. pp. 363.

Guisan, A., S.B. Weiss, and A.D. Weiss. 1999. GLM versus CCA spatial modeling of plant species distribution. *Plant Ecol.* **143**, 107–122.

Gultepe, I., R. Tardif, S.C. Michaelides, J. Cermak, A. Bott, J. Bendix, M.D. Müller, M. Pagowski, B. Hansen, G. Ellrod, W. Jacobs, G. Toth, and S.G. Cober. 2007. Fog Research: A Review of Past Achievements and Future Perspectives. *Pure Appl. Geophys.* **164**, 1121–1159. https://10.1007/s00024-007-0211-x.

Hang, C., D.F. Nadeau, I. Gultepe, S.W. Hoch, C. Román-Cascón, K. Pryor, H.J.S. Fernando, E.D. Creegan, L.S. Leo, Z. Silver, and E.R. Pardyjak. 2016. A Case Study of the Mechanisms Modulating the Evolution of Valley Fog. *Pure Appl. Geophys.* **173**, 3011–3030. https://10.1007/s00024-016-1370-4.

Hesse, R. 2012. Spatial distribution of and topographic controls on Tillandsia fog vegetation in coastal southern Peru : Remote sensing and modelling. *J. Arid Environ.* **78**, 33–40. https://10.1016/j.jaridenv.2011.11.006.

Hildebrandt, A., M. Al Aufi, M. Amerjeed, M. Shammas, and E.A.B. Eltahir. 2007. Ecohydrology of a seasonal cloud forest in Dhofar: 1. Field experiment. *Water Resour. Res.* **43**, 1–13. https://10.1029/2006WR005261.

Hildebrandt, A., and E.A.B. Eltahir. 2006. Forest on the edge: Seasonal cloud forest in Oman

creates its own ecological niche. *Geophys. Res. Lett.* **33**, 2–5. https://10.1029/2006GL026022.

Hildebrandt, A., and E.A.B. Eltahir. 2007. Ecohydrology of a seasonal cloud forest in Dhofar: 2. Role of clouds, soil type, and rooting depth in tree-grass competition. *Water Resour. Res.* **43**, 1–13. https://10.1029/2006WR005262.

Hildebrandt, A., and E.A.B. Eltahir. 2008. Using a horizontal precipitation model to investigate the role of turbulent cloud deposition in survival of a seasonal cloud forest in Dhofar. *J. Geophys. Res.* **113**, 1–11. https://10.1029/2008JG000727.

Kidron, G.J. 2005. Angle and aspect dependent dew and fog precipitation in the Negev desert. *J. Hydrol.* **301**, 66–74. https://10.1016/j.jhydrol.2004.06.029.

Kürschner, H., P. Hein, N. Kilian, and M.A. Hubaishan. 2004. The Hybantho durae-Anogeissetum dhofaricae ass. nova - Phytosociology, structure and ecology of an endemic South Arabian forest community. *Phytocoenologia*. **34**, 569–612. https://10.1127/0340-269X/2004/0034-0569.

Lawton, R.M. 1978. A reconnaissance survey of the Jebel Qara grazing land ecosystem, with particular reference to the impact of development. Ministry of Overseas Development, Surbiton. pp. 46.

Lehnert, L.W., B. Thies, K. Trachte, S. Achilles, P. Osses, K. Baumann, J. Schmidt, E. Samolov, P. Jung, P. Leinweber, U. Karsten, B. Büdel, and J. Bendix. 2018. A case study on fog/low stratus occurrence at las lomitas, atacama desert (Chile) as a water source for biological soil crusts. *Aerosol Air Qual. Res.* **18**, 254–269. https://10.4209/aaqr.2017.01.0021.

Martorell, C., and E. Ezcurra. 2002. Rosette scrub occurrence and fog availability in arid mountains of Mexico. *J. Veg. Sci.* **13**, 651–662. https://10.1111/j.1654-1103.2002.tb02093.x.

Meister, J., M.A. Hubaishan, N. Kilian, and C. Oberprieler. 2005. Chloroplast DNA variation in the shrub Justicia areysiana (Acanthaceae) endemic to the monsoon affected coastal mountains of the southern Arabian Peninsula. *Bot. J. Linn. Soc.* **148**, 437–444.

Miller, A., M. Morris, and S. Stuart-Smith. 1988. Plants of Dhofar, The Southern Region of Oman: Traditional, Economic, and Medicinal Uses. Office of the Adviser for Conservation of the Environment, Diwan of Royal Court, Muscat. pp. 390.

Miska, L., and H. Jan. 2004. Evaluation of current statistical approaches for predictive geomorphological mapping. *Geomorphology*. **67**, 299–315. https://10.1016/j.geomorph.2004.10.006.

Mittermeier, R.A., P.R. Gil, M. Hoffman, J. Pilgrim, T. Brooks, C.G. Mittermeier, G.A.B. da Fonseca, and J. Lamoreux. 2004. Hotspots Revisited: Earth's Biologically Richest and Most Endangered Terrestrial Ecoregions. R.A. Mittermeier, editor. CEMEX, Rugby. pp. 390.

Moore, I.D., R.B. Grayson, and A.R. Ladson. 1991. Digital Terrain Modelling: A review of hydrological, geomorphological, and biological applications. *Hydrol. Process.* **5**, 3–30. https://https://doi.org/10.1002/hyp.3360050103.

Mosti, S., M. Raffaelli, and M. Tardelli. 2012. Contribution to the Flora of Central-Southern Dhofar (Sultanate of Oman). *Webbia*. **67**, 65–91. https://10.1080/00837792.2012.10670909.

Mulligan, M. 2010. Modelling the tropics-wide extent and distribution of cloud forests and cloud forest loss with implications for their conservation priority. *In* Tropical Montane Cloud Forests: Science for Conservation and Management. L.A. Bruijnzeel, F.N. Scatena, and L.S. Hamilton, editors. Cambridge University Press, Cambridge. 14–38.

Obregon, A., C. Gehrig-Downie, S.R. Gradstein, and J. Bendix. 2014. The potential distribution of tropical lowland cloud forest as revealed by a novel MODIS-based fog/low stratus night-time detection scheme. *Remote Sens. Environ.* **155**, 312–324.

https://10.1016/j.rse.2014.09.005.

Patzelt, A. 2011. The Themeda Quadrivalvis Tall-Grass Savannah of Oman at the Crossroad Between Africa and Asia. *Edinburgh J. Bot.* **68**, 301–319. https://10.1017/S0960428611000217.

Patzelt, A. 2015. Synopsis of the Flora and Vegetation of Oman, with Special Emphasis on Patterns of Plant Endemism. *Abhandlungen der Braunschw. Wissenschaftlichen Gesellschaft*. 282–317.

Patzelt, A., L. Morris, L. Al Harthi, I. Al Rashdi, and A. Spalton. 2008. The Oman Botanic Garden (1): The Vision, early plant collections and propagation. *Sibbaldia*. **6**, 41–77.

Patzelt, A., L.M. Morris, K. Al Farsi, and A. Spalton. 2009. The Oman Botanic Garden (2): Collections Policy, Nursery Construction, Expanded Plant Production and Initial Tree Translocation. *Sibbaldia*. **7**, 83–97.

Pike, R.J., and S.E. Wilson. 1971. Elevation-Relief Ratio, Hypsometric Integral, and Geomorphic Area-Altitude Analysis. *Geol. Soc. Am. Bull.* **82**, 1079–1084.

Prasad, A.M., L.R. Iverson, and A. Liaw. 2006. Newer classification and regression tree techniques: Bagging and random forests for ecological prediction. *Ecosystems*. **9**, 181–199. https://10.1007/s10021-005-0054-1.

R Core team. 2019. R: A language and environment for statistical computing. R Foundation for Statistical Computing, Vienna, Austria.

Raffaelli, M., and M. Tardelli. 2006. Phytogeographic zones of Dhofar (Southern Oman). *Bocconea*. **19**, 103–108.

Riley, S., S. DeGloria, and R. Elliot. 1999. A terrain ruggedness index that quantifies topographic heterogeneity. *Intermt. J. Sci.* **5**, 23–27.

Roberts, D.W., and S. V Cooper. 1989. Concepts and techniques of vegetation mapping. USDA Forest Service, Washington. pp. 96.

Rouse, J.W., R.H. Haas, J.A. Schell, and D.W. Deering. 1974. Monitoring vegetation systems in the great plains with ERTS. *Proc. Third Earth Resour. Technol. Satell. Symp.* **1**, 309–317.

Scholte, P., and P. De Geest. 2010. The climate of Socotra Island (Yemen): A first-time assessment of the timing of the monsoon wind reversal and its influence on precipitation and vegetation patterns. *J. Arid Environ.* **74**, 1507–1515. https://10.1016/j.jaridenv.2010.05.017.

Sousa, D., C. Small, A. Spalton, and A. Kwarteng. 2019. Coupled spatiotemporal characterization of monsoon cloud cover and vegetation phenology. *Remote Sens.* **11**, 1–22. https://10.3390/rs11101203.

Spalton, A., and H. Al Hikmani. 2014. The Arabian Leopards of Oman. 1st ed. Stacey International, London. pp. 160.

Spruill, T.B., W.J. Showers, and S.S. Howe. 2010. Application of Classification-Tree Methods to Identify Nitrate Sources in Ground Water. *J. Environ. Qual.* **31**, 1538. https://10.2134/jeq2002.1538.

Stanley Price, M.R., A.H. Al-Harthy, and R.P. Whitcombe. 1988. Fog moisture and its ecological effects in Oman. *In* Arid Lands: Today and Tomorrow. E.E. Whitehead, C.F. Hutchinson, B.N. Timmermann, and R.G. Varady, editors. Westview Press, Boulder, Colorado. 69–88.

Therneau, T., and E. Atkinson. 2019a. rpart: Recursive Partitioning and Regression Trees.

Therneau, T., and E. Atkinson. 2019b. An Introduction to Recursive Partitioning Using the RPART Routines. Mayo Foundation, Scottsdale. pp. 1–60.

Thuiller, W., J. Vayreda, J. Pino, S. Sabate, S. Lavorel, and C. Gracia. 2003. Large-scale environmental correlates of forest tree distributions in Catalonia (NE Spain). *Glob. Ecol. Biogeogr.* **12**, 313–325. https://10.1046/j.1466-822X.2003.00033.x.

Tian, S., A.I.J.M. Van Dijk, P. Tregoning, and L.J. Renzullo. 2019. Forecasting dryland vegetation condition months in advance through satellite data assimilation. *Nat. Commun.* **10**, 1–7. https://10.1038/s41467-019-08403-x.

Walmsley, J.L., R.S. Schemenauer, and H.A. Bridgman. 1996. A method for estimating the hydrologic input from fog in mountainous terrain. *J. Appl. Meteorol.* **35**, 2237–2249. https://https://doi.org/10.1175/1520-0450(1996)035<2237:AMFETH>2.0.CO;2.

Wang, B., A. Ono, K. Muramatsu, and N. Fujiwarattt. 1999. Automated detection and removal of clouds and their shadows from landsat TM images. *IEICE Trans. Inf. Syst.* **E82–D**, 453–460.

Weathers, K.C., S.M. Simkin, G.M. Lovett, and S.E. Lindberg. 2006. Empirical modeling of atmospheric deposition in mountainous landscapes. *Ecol. Appl.* **16**, 1590–1607. https://10.1890/1051-0761(2006)016[1590:EMOADI]2.0.CO;2.

Zuhlke, M., N. Fomferra, C. Brockmann, M. Peters, L. Veci, J. Malik, and P. Regner. 2015. SNAP (Sentinel Application Platform) and the ESA Sentinel 3 Toolbox. ESA, Paris. pp. 21.